Particle pressure, inertial force, and ring current density profiles in the magnetosphere of Saturn, based on Cassini measurements

N. Sergis,[1] S. M. Krimigis,[1,2] E. C. Roelof,[2] C. S. Arridge,[3,9] A. M. Rymer,[2] D. G. Mitchell,[2] D. C. Hamilton,[4] N. Krupp,[5] M. F. Thomsen,[6] M. K. Dougherty,[7] A. J. Coates,[3,9] and D. T. Young[8]

Received 25 November 2009; accepted 14 December 2009; published 20 January 2010.

[1] We report initial results on the particle pressure distribution and its contribution to ring current density in the equatorial magnetosphere of Saturn, as measured by the Magnetospheric Imaging Instrument (MIMI) and the Cassini Plasma Spectrometer (CAPS) onboard the Cassini spacecraft. Data were obtained from September 2005 to May 2006, within ±0.5 R_S from the nominal magnetic equator in the range 6 to 15 R_S. The analysis of particle and magnetic field measurements, the latter provided by the Cassini magnetometer (MAG), allows the calculation of average radial profiles for various pressure components in Saturn's magnetosphere. The radial gradient of the total particle pressure is compared to the inertial body force to determine their relative contribution to the Saturnian ring current, and an average radial profile of the azimuthal current intensity is deduced. The results show that: (1) Thermal pressure dominates from 6 to 9 R_S, while thermal and suprathermal pressures are comparable outside 9 R_S with the latter becoming larger outside 12 R_S. (2) The plasma β (particle/magnetic pressure) remains $\geq$1 outside 8 R_S, maximizing ($\sim$3 to $\sim$10) between 11 and 14 R_S. (3) The inertial body force and the pressure gradient are similar at 9–10 R_S, but the gradient becomes larger $\geq$11 R_S. (4) The azimuthal ring current intensity develops a maximum between approximately 8 and 12 R_S, reaching values of 100–150 pA/m^2. Outside this region, it drops with radial distance faster than the 1/r rate assumed by typical disk current models even though the total current is not much different to the model results. **Citation:** Sergis, N., et al. (2010), Particle pressure, inertial force, and ring current density profiles in the magnetosphere of Saturn, based on Cassini measurements, *Geophys. Res. Lett.*, *37*, L02102, doi:10.1029/2009GL041920.

1. Introduction

[2] The Saturnian ring current was initially inferred from magnetic field [*Connerney et al.*, 1981, 1983] and particle [*Krimigis et al.*, 1981, 1983; *Mauk et al.*, 1985] measurements during the Voyager 1 and 2 flybys, and studied in more detail with Cassini [*Krimigis et al.*, 2007; *Sergis et al.*, 2007, 2009; *Arridge et al.*, 2007, 2008; *Brandt et al.*, 2008; *Kellett et al.*, 2009].

[3] The planetary ring current is located between $\sim$8 and $\sim$18 R_S (R_S = 60268 km), in a region where plasma is slowed with respect to corotation [*Wilson et al.*, 2008; *McAndrews et al.*, 2009], primarily composed of O^+ ions and characterized by increased suprathermal (>3 keV) particle pressure with high (>1) plasma β and intense dynamic behavior. The physical mechanisms, however, governing the characteristics and dynamics of the ring current are not fully understood. *Bunce et al.* [2007] studied the ring current using magnetic field measurements and an axisymmetric model [*Connerney et al.*, 1983], arguing that the ring current is dominated by inertial currents. *Sergis et al.* [2009] showed that the average radial suprathermal pressure gradient is sufficient to modify the radial force balance and the azimuthal current.

[4] Since July 1 2004, Cassini is orbiting Saturn and monitors its magnetospheric environment via in-situ and remote measurements. In this study we combine particle data with magnetic field measurements for radial distances between 6 and 15 R_S. Energetic particles are sampled by the Charge Energy Mass Spectrometer (CHEMS) sensor of the Magnetospheric Imaging Instrument (MIMI) [*Krimigis et al.*, 2004]. *Sergis et al.* [2009] have shown that the observed intensities are generally representative of the energetic particle intensity perpendicular to the local magnetic field. The magnetic field vector is measured by Cassini's fluxgate magnetometer [*Dougherty et al.*, 2004].

[5] Plasma properties are measured with the ion mass spectrometer (IMS) and the electron spectrometer (ELS), parts of the Cassini plasma spectrometer (CAPS) [*Young et al.*, 2004]. The IMS measures ions between 1 eV/e and 50 keV/e while the ELS has a measurement range of 0.6 eV/e to 28 keV/e. Both sensors are mounted on an actuating platform providing directional flux measurements.

[6] Since the field-of-view (FOV) pointing of the CAPS sensors depends on the orientation of the spacecraft, it is not always possible to measure plasma quantities such as pitch

[1]Office for Space Research and Technology, Academy of Athens, Athens, Greece.
[2]Applied Physics Laboratory, Johns Hopkins University, Laurel, Maryland, USA.
[3]Mullard Space Science Laboratory, University College London, Dorking, UK.
[4]Department of Physics, University of Maryland, College Park, Maryland, USA.
[5]Max-Planck-Institut für Sonnensystemforschung, Lindau, Germany.
[6]Los Alamos National Laboratory, Los Alamos, New Mexico, USA.
[7]Space and Atmospheric Physics Group, Imperial College, London, UK.
[8]Division of Space Science and Engineering, Southwest Research Institute, San Antonio, Texas, USA.
[9]Centre for Planetary Sciences, Birkbeck, University College London, London, UK.

0094-8276/10/2009GL041920$05.00

angle distributions or flow velocity, thus limiting the calculation of plasma moments determined by forward modeling techniques [e.g., *Lewis et al.*, 2008; *Wilson et al.*, 2008] to a subset of available data. For the present study we have employed plasma moments that were calculated based on numerical integration of the observed IMS singles (SNG) count rates for times when the nominal plasma corotation flow direction was in the FOV of the IMS, and for which no warning flags were set (cf., M. F. Thomsen et al., 2009, in preparation). In addition, we have included the inner magnetosphere parameter set derived by forward modeling [*Wilson et al.*, 2008] and those for the tail region [*McAndrews et al.*, 2009].

[7] The CAPS and MIMI ion sensors overlap between 3 and 45 keV. However, the amount of actual double bookkeeping does not correspond to the full range of this overlap, mostly due to the different geometrical factors and sensitivity of the two sensors and the average spectral shape in the regions of interest. Our analysis of typical spectra suggests that the resulting overestimation of the total plasma pressure is <25% and is well masked by the natural scatter in the data.

[8] The availability of ion plasma moments and the existing suprathermal pressure profile [*Sergis et al.*, 2009] offer for the first time the opportunity of computing the total particle pressure. In this study we present radial profiles for the pressure components in the equatorial magnetosphere of Saturn, expanding previous works by *Sergis et al.*, [2007, 2009], and *Wilson et al.* [2008]. The results reveal an azimuthal current with maximum intensity of 100–150 pA/m^2, primarily due to the plasma pressure gradient. We note that energetic neutral atom (ENA) images obtained by the ion and neutral camera (INCA) of MIMI show that the instantaneous ring current is non-uniform (partial ring current) [e.g., *Carbary et al.*, 2008], indicating that any study utilizing long term measurements can only depict the average state of the middle magnetosphere and likely underestimate peaks in the ring current. Moreover, the fact that most of the magnetospheric parameters (density, pressure, ENA emission, magnetic field) are longitude dependent imposes an a-priori limitation to any symmetric ring current model. A detailed study addressing orbit-to-orbit variability in the ring current including comparison with model predictions for the radial dependence of the current density is currently in preparation by *S. Kellett et al.* [2010].

2. Results

[9] The radial profile for different pressure components in the Saturnian magnetosphere is shown in Figure 1a. It is evident that, despite significant scatter in the data, the thermal plasma pressure is dominant for r $\leq$ 9 R_S, while the suprathermal pressure progressively prevails for r $\geq$ 12 Rs. The thermal electron pressure remains lower than the ion pressures by a factor of $\sim$10. *Schippers et al.* [2008] showed that during one pass the suprathermal electron pressure was significant between 9 and 15 R_S, compared to the average shown in Figure 1a. A direct comparison during that pass (not presented here), showed the ion pressure to be higher than the average shown. Thus, neglecting the suprathermal electron pressure is not expected to significantly affect our conclusions. The total particle pressure (panel b) is relatively flat between 6 and 8 R_S with typical values close to 0.4 nPa, but drops by $\times$10 by 15 R_S. The total particle pressure is almost equal to the measured magnetic pressure ($\beta \approx 1$) near 8 R_S, while beyond 9 R_S the particle pressure dominates with β reaching values of 3 to 10 between 11 and 14 R_S. A high β regime in this region was also reported by *Sergis et al.* [2009], with lower, however, values, as it did not include the thermal plasma pressure, while *Sittler et al.* [2008] also reported a thermal plasma pressure close to the magnetic pressure near the distance of Rhea (8.7 R_S), based on measurements from the Saturn Orbit Insertion (SOI).

[10] The radial profile of the total particle pressure indicates that its decay region (r > 7 R_S) is characterized by a significant (negative) gradient. Assuming that the plasma is corotating with constant angular velocity and all ion components have the same bulk velocity, the radial, steady-state form of the force balance equation in the equatorial plane can be written as:

$$\rho \frac{V_\phi^2}{r} - \frac{\partial P}{\partial r} - \frac{P_\perp}{R_C}\left(\frac{A-1}{A}\right) \approx J_\phi B_z \quad (1)$$

with ρ the plasma mass density, V_φ the in-situ measured azimuthal flow velocity, P the total particle pressure, $P_\perp$ the field perpendicular thermal pressure component, R_C the curvature of the field lines, A the thermal plasma pressure anisotropy ($A = P_\perp/P_{/\!/}$, $P_{/\!/}$ being the parallel thermal pressure), J_φ the azimuthal current density and B_z the magnetic field component normal to the nominal equatorial plane. The 3 terms on the left side represent the inertial, the pressure gradient and the pressure anisotropy components of the force in the radial direction. When solving for J_φ, equation (1) becomes:

$$J_\phi \approx \frac{1}{B_z}\left(\rho \frac{V_\phi^2}{r} - \frac{\partial P}{\partial r} - \frac{P_\perp}{R_C}\left(\frac{A-1}{A}\right)\right) \quad (2)$$

[11] Figure 1c shows the radial profile of the inertial body force $\rho(V_\varphi^2/r)$ (see also Thomsen et al. in preparation) with an exponential fit to the measured data and dashed lines to represent a 1-σ zone of the distribution. This profile is shown together with the particle pressure gradient ($-\frac{\partial P}{\partial r}$) and the anisotropy force $F_A = -\frac{P_\perp}{R_C}\left(\frac{A-1}{A}\right)$ in Figure 1d, illustrating their relative contribution to the ring current vs. radial distance. The anisotropy force was directly calculated (and consecutively fitted) from the thermal pressure anisotropy measurements available for 6 to 10 R_S [*Wilson et al.*, 2008]. Analysis of long term magnetic field measurements shows that for these radial distances the dipole approximation can be safely used to determine the magnetic curvature as R_C = r/3. The pressure radial gradient comes from differentiating the polynomial fit (Figure 1b) to the total particle pressure. Inside $\sim$9 R_S (neutral cloud) the anisotropy force is significant, but remains lower by a factor of 2 to 3 compared to the inertial body force which prevails due to the higher mass density and plasma angular velocity in that region. Between 9 and 10 R_S the inertial and pressure

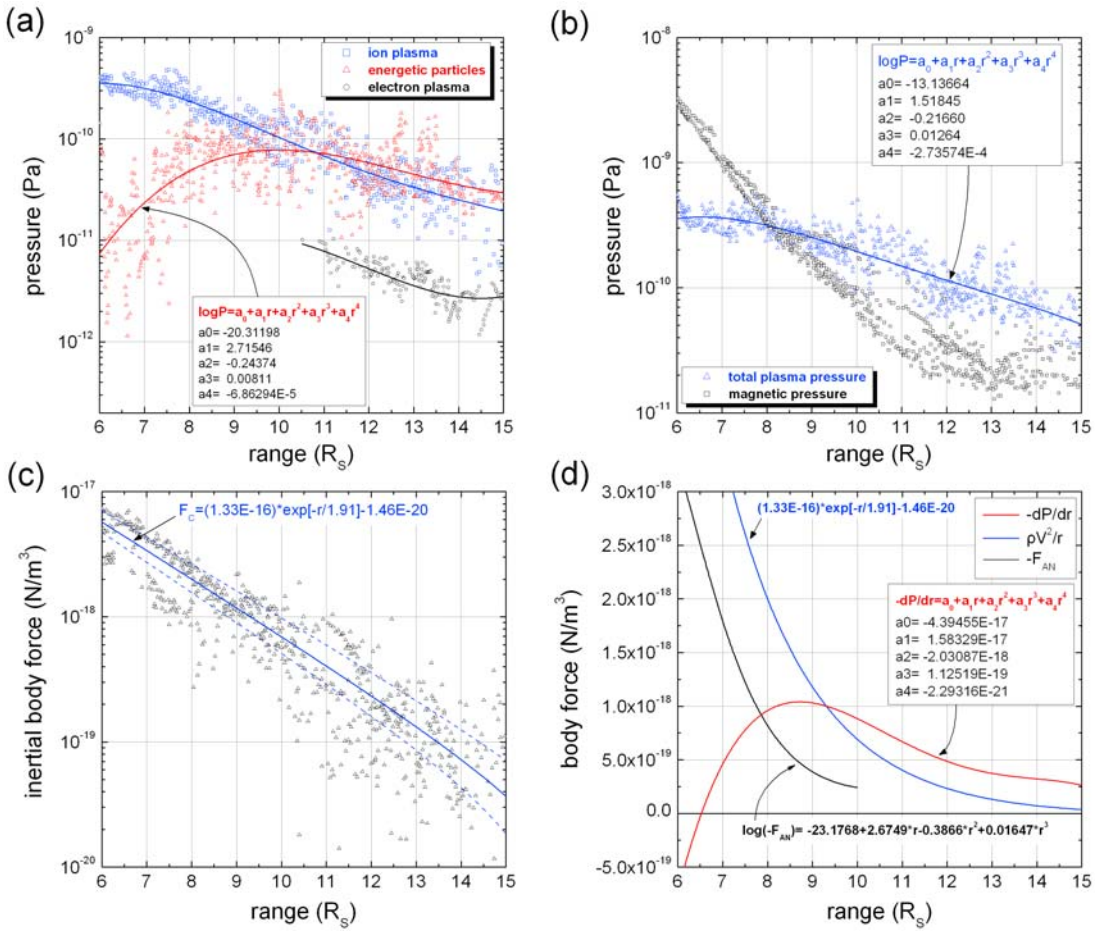

Figure 1. (a) Radial pressure profile for thermal ion plasma (blue), energetic particles (red), and thermal electron plasma (black), together with polynomial fits of the same color. The apparent scatter is indicative of the intense dynamics present in the Saturnian magnetosphere. Electron moments are not available inside 10 R_S due to the spacecraft potential noise. (b) Radial profiles for the magnetic pressure (black) and the total particle pressure (blue), with a polynomial fit of the same colors. (c) Radial dependence of the inertial body force. The blue solid line is an exponential fit to the data, while dashed lines bracket a 1-σ zone of the distribution. (d) Radial profiles of the inertial body force (blue), the particle pressure gradient (red) and the pressure anisotropy force (black). The blue line is the exponential fit shown in Figure 1c, the red line is the derivative of the polynomial fit to the total pressure (shown in Figure 1b).

gradient terms are comparable, while further out the latter becomes greater by a factor of 2 to 5, indicating that in this part of the magnetosphere, the ring current is primarily pressure gradient-driven and modified by the energetic particle population, especially during injection events [*Mauk et al.*, 2005; *Paranicas et al.*, 2007], when the suprathermal pressure is significantly increased and the local mass density is lower.

[12] Having all components of equation (2) either directly measured or derived from the data permits the calculation of the corresponding ring current density. In Figure 2a the inertial, the pressure gradient and the pressure anisotropy components of J_φ are shown. Inertial and pressure gradient currents are similar between 9 and 10 R_S; beyond that range the inertial ring current drops quickly. The increased scatter for $r > 10$ R_S is primarily due to fluctuations in the suprathermal pressure.

[13] The total ring current density profile is presented in Figure 2b together with an $r^{-2.2}$ function that describes quite well the decrease of the measured ring current density for $r > 11$ R_S. The red dashed line (dotted for $r > 10$ R_S) shows the total current density when the anisotropy current is included. The estimates of the inertial ring current from the model of *Connerney et al.* [1983] (Voyager measurements) and *Bunce et al.* [2007] (Cassini measurements) are also shown. The measured ring current density develops a maximum region between 8 and 12 R_S, not predicted by either model, but in agreement with *Mauk et al.* [1985] and *Beard and Gast* [1987, Figure 3], reaching values of 100–150 pA/m^2. As evident from Figure 2a, this maximum J_φ region is imposed by the pressure gradient.

[14] It is interesting to examine under what conditions (i.e. relative magnitudes of $\rho\frac{V_\phi^2}{r}$ and $-\frac{\partial P}{\partial r}$) a maximum in J_φ develops. Figure 3 is a parametric study of the radial profile of the total J_φ for different (lower) values of particle pressure gradient, while the inertial term is kept constant. The maximum in the ring current starts forming for pressure gradient even 4 times smaller than that measured, indicating

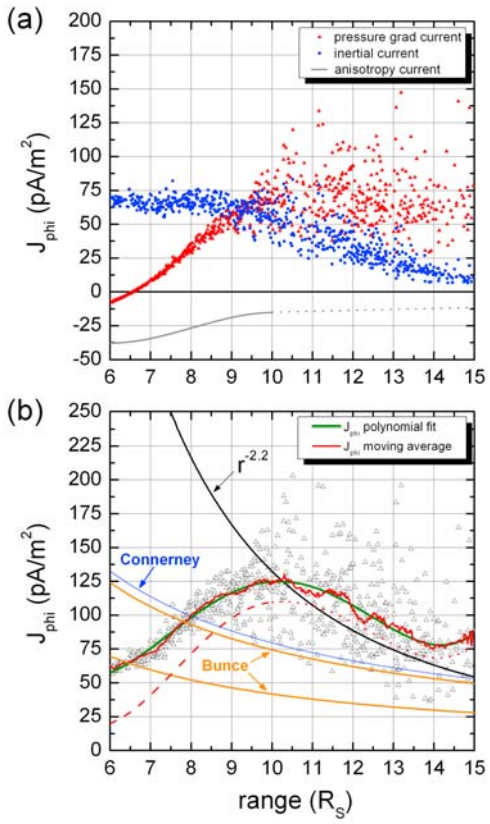

Figure 2. (a) Radial profiles for the inertial ($\frac{1}{B_Z}\rho\frac{V_\phi^2}{r}$), the pressure gradient ($-\frac{1}{B_Z}\frac{\partial P}{\partial r}$), and the pressure anisotropy $-\frac{P_\perp}{B_Z R_C}\left(\frac{A-1}{A}\right)$ contribution to the total current density J_φ in blue, red, and gray (solid for the measured, dotted for the extrapolated part), respectively. The ring current progressively changes from purely inertial inside of 8 R_S, to pressure gradient-driven for $r \geq 11$ R_S. (b) Radial profile of the total ring current density J_φ. The red line is a moving average, the green line is a polynomial fit to the data, while the black line represents an $r^{-2.2}$ power low. The blue line is the J_φ output of the *Connerney et al.* [1983] model (Voyager data) and the orange lines correspond to the min and max J_φ profiles produced by *Bunce et al.* [2007] (Cassini data). The red dashed line (dotted for $r > 10$ R_S) is the total current density if the pressure anisotropy current is included.

that the ring current is strongly affected by the particle pressure even during times of moderate magnetospheric activity.

3. Summary and Discussion

[15] The key questions that this study addresses are: (1) What is the radial profile of each pressure component in the equatorial magnetosphere of Saturn? How do different pressures compare for different radial distances? (2) Can we determine if the azimuthal ring current J_φ is inertial, pressure gradient-driven or a combination of both? What is its radial dependence?

[16] Plasma, energetic particle and magnetic field measurements by Cassini used to calculate the total particle pressure and its radial gradient for a large part of the equatorial magnetosphere show that: (1) Typical values of the particle pressure are 0.4 nPa (6 R_S) dropping to 0.05 nPa (15 R_S), with plasma $\beta > 1$ outside 8 R_S and maximum values of ~3 to 10 between 11 and 14 R_S. (2) The contribution of the energetic particles to the total particle pressure becomes significant at >9 R_S and progressively overtakes the thermal plasma beyond 12 R_S. (3) The inertial body force and the radial pressure gradient (and consequently their contribution to J_φ) are comparable at 9–10 R_S with the pressure gradient becoming greater outside of 11 R_S, while the inertial force prevails inside 8.5 R_S. (4) Inclusion of the anisotropy current (dashed and dotted curves in Figure 2b) affects the total current mostly in the inner part (~60% maximum decrease at 6 R_S) compared to the maximum region (~10% at 10 R_S). The shape of the J_φ profile does not change noticeably. (5) The ring current density develops a maximum between 8 and 12 R_S reaching values of 100–150 pA/m^2, in the same region where maximum ENA emission has been observed [*Carbary et al.*, 2008] and suprathermal electron pressure increases, with electron β~1 [*Schippers et al.*, 2008]. Outside this region, J_φ drops with radial distance much faster than the 1/r dependence that disk current models assume ($J_\varphi \propto r^{-2.2}$ outside ~10 Rs). Further analysis indicates that the maximum in J_φ would be present even for a considerably lower (factor of 3 to 4) pressure gradient (moderate magnetospheric activity), while the 1/r decrease does not represent the data well for any relative strength of the terms contributing to J_φ. As the suprathermal electron pressure is not included in our study (not yet available for more than one orbit), the pressure gradient deduced here could be somewhat underestimated.

[17] Our results confirm that Saturn possesses an intense and variable ring current, which is primarily inertial at <8.5 R_S but increasingly pressure gradient-driven in its maximum region (8 to 12 R_S) and certainly farther out. This fact needs to be accounted for, when modeling the magnetosphere-ionosphere coupling (mapping the magnetospheric regions into the ionosphere). The predictions of certain disk models [e.g., *Connerney et al.*, 1983; *Bunce*

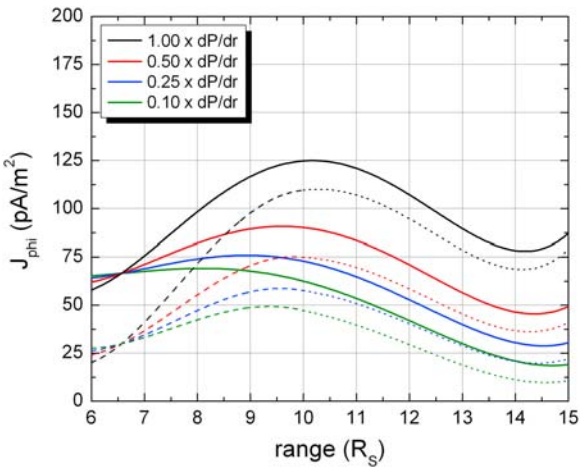

Figure 3. Total ring current density profiles for different contributions of the pressure gradient term (0.1, 0.25, 0.5, and 1.0 of the measured $-\frac{\partial P}{\partial r}$, in green, blue, red, and black, respectively). The dash-dotted lines show the same results if the anisotropy current is included.

et al., 2007] are consistent with the deduced total current, but cannot describe successfully the ring current radial density profile as observed by Cassini.

[18] **Acknowledgments.** We thank M. Kusterer (JHU/APL) for assistance with the data reduction. We are grateful to MIMI colleagues for comments that improved this study. We also thank R.J. Wilson and H.J. McAndrews for ion moment calculations. Work at JHU/APL was supported by NASA and by subcontracts at the UMD and the Academy of Athens. The German contribution of MIMI/LEMMS was financed by the Bundesministerium für Bildung und Forschung through the Deutsches Zentrum für Luft und Raumfahrt and by the Max-Planck-Gesellschaft. C.S.A. and A.J.C. were funded in the UK by the Science and Technology Facilities Council rolling grant to MSSL/UCL. Cassini CAPS/ELS data processing is funded in the UK by STFC. Work at LANL was conducted under the auspices of the U.S. Dep. of Energy, with support from the NASA Cassini project.

References

Arridge, C. S., C. T. Russell, K. K. Khurana, N. Achilleos, N. André, A. M. Rymer, M. K. Dougherty, and A. J. Coates (2007), Mass of Saturn's magnetodisc: Cassini observations, *Geophys. Res. Lett.*, *34*, L09108, doi:10.1029/2006GL028921.

Arridge, C. S., C. T. Russell, K. K. Khurana, N. Achilleos, S. W. H. Cowley, M. K. Dougherty, D. J. Southwood, and E. J. Bunce (2008), Saturn's magnetodisc current sheet, *J. Geophys. Res.*, *113*, A04214, doi:10.1029/2007JA012540.

Beard, D. B., and M. A. Gast (1987), The magnetosphere of Saturn, *J. Geophys. Res.*, *92*, 5763–5767, doi:10.1029/JA092iA06p05763.

Brandt, P., C. P. Paranicas, J. F. Carbary, D. G. Mitchell, B. H. Mauk, and S. M. Krimigis (2008), Understanding the global evolution of Saturn's ring current, *Geophys. Res. Lett.*, *35*, L17101, doi:10.1029/2008GL034969.

Bunce, E. J., S. W. H. Cowley, I. I. Alexeev, C. S. Arridge, M. K. Dougherty, J. D. Nichols, and C. T. Russell (2007), Cassini observations of the variation of Saturn's ring current parameters with system size, *J. Geophys. Res.*, *112*, A10202, doi:10.1029/2007JA012275.

Carbary, J. F., D. G. Mitchell, P. Brandt, E. C. Roelof, and S. M. Krimigis (2008), Statistical morphology of ENA emissions at Saturn, *J. Geophys. Res.*, *113*, A05210, doi:10.1029/2007JA012873.

Connerney, J. E. P., M. H. Acuña, and N. F. Ness (1981), Saturn's ring current and inner magnetosphere, *Nature*, *292*, 724–726, doi:10.1038/292724a0.

Connerney, J. E. P., M. H. Acuña, and N. F. Ness (1983), Currents in Saturn's magnetosphere, *J. Geophys. Res.*, *88*, 8779–8789, doi:10.1029/JA088iA11p08779.

Dougherty, M. K., et al. (2004), The Cassini Magnetic Field Investigation, *Space Sci. Rev.*, *114*(1–4), 331–383, doi:10.1007/s11214-004-1432-2.

Kellett, S., E. J. Bunce, A. J. Coates, and S. W. H. Cowley (2009), Thickness of Saturn's ring current determined from north–south Cassini passes through the current layer, *J. Geophys. Res.*, *114*, A04209, doi:10.1029/2008JA013942.

Krimigis, S. M., et al. (1981), Low-energy charged particles in Saturn's magnetosphere: Results from Voyager 1, *Science*, *212*, 225–231, doi:10.1126/science.212.4491.225.

Krimigis, S. M., J. F. Carbary, E. P. Keath, T. P. Armstrong, L. J. Lanzerotti, and G. Gloeckler (1983), General characteristics of hot plasma and energetic particles in the Saturnian magnetosphere: Results from the Voyager spacecraft, *J. Geophys. Res.*, *88*, 8871–8892, doi:10.1029/JA088iA11p08871.

Krimigis, S. M., et al. (2004), Magnetosphere Imaging Instrument (MIMI) on the Cassini Mission to Saturn/Titan, *Space Sci. Rev.*, *114*, 233–329, doi:10.1007/s11214-004-1410-8.

Krimigis, S. M., N. Sergis, D. G. Mitchell, D. C. Hamilton, and N. Krupp (2007), A dynamic, rotating ring current around Saturn, *Nature*, *450*(7172), 1050–1053, doi:10.1038/nature06425.

Lewis, G. R., N. André, C. S. Arridge, A. J. Coates, L. K. Gilbert, D. R. Linder, and A. M. Rymer (2008), Derivation of density and temperature from the Cassini Huygens CAPS electron spectrometer, *Planet. Space Sci.*, *56*(7), 901–912, doi:10.1016/j.pss.2007.12.017.

Mauk, B. H., S. M. Krimigis, and R. P. Lepping (1985), Particle and field stress balance within a planetary magnetosphere, *J. Geophys. Res.*, *90*, 8253–8264, doi:10.1029/JA090iA09p08253.

Mauk, B. H., et al. (2005), Energetic particle injections in Saturn's magnetosphere, *Geophys. Res. Lett.*, *32*(14), L14S05, doi:10.1029/2005GL022485.

McAndrews, H. J., et al. (2009), Plasma in Saturn's night side magnetosphere and the implications for global circulation, *Planet. Space Sci.*, *57*, 1714–1722, doi:10.1016/j.pss.2009.03.003.

Paranicas, C. P., D. G. Mitchell, E. C. Roelof, B. H. Mauk, S. M. Krimigis, P. C. Brandt, M. Kusterer, F. S. Turner, J. Vandegriff, and N. Krupp (2007), Energetic electrons injected into Saturn's neutral gas cloud, *Geophys. Res. Lett.*, *34*, L02109, doi:10.1029/2006GL028676.

Schippers, P., et al. (2008), Multi-instrument analysis of electron populations in Saturn's magnetosphere, *J. Geophys. Res.*, *113*, A07208, doi:10.1029/2008JA013098.

Sergis, N., S. M. Krimigis, D. G. Mitchell, D. C. Hamilton, N. Krupp, B. M. Mauk, E. C. Roelof, and M. Dougherty (2007), Ring current at Saturn: Energetic particle pressure in Saturn's equatorial magnetosphere measured with Cassini/MIMI, *Geophys. Res. Lett.*, *34*, L09102, doi:10.1029/2006GL029223.

Sergis, N., S. M. Krimigis, D. G. Mitchell, D. C. Hamilton, N. Krupp, B. H. Mauk, E. C. Roelof, and M. K. Dougherty (2009), Energetic particle pressure in Saturn's magnetosphere, measured with Magnetospheric Imaging Instrument on Cassini, *J. Geophys. Res.*, *114*, A02214, doi:10.1029/2008JA013774.

Sittler, E. C., et al. (2008), Ion and neutral sources and sinks within Saturn's inner magnetosphere: Cassini results, *Planet. Space Sci.*, *56*, 3–18, doi:10.1016/j.pss.2007.06.006.

Wilson, R. J., R. L. Tokar, M. G. Henderson, T. W. Hill, M. F. Thomsen, and D. H. Pontius Jr. (2008), Cassini Plasma Spectrometer Thermal Ion Measurements in Saturn's Inner Magnetosphere, *J. Geophys. Res.*, *113*, A12218, doi:10.1029/2008JA013486.

Young, D. T., et al. (2004), Cassini Plasma Spectrometer Investigation, *Space Sci. Rev.*, *114*(1–4), 1–112, doi:10.1007/s11214-004-1406-4.

C. S. Arridge and A. J. Coates, Mullard Space Science Laboratory, University College London, Dorking RH5 6NT, UK.

M. K. Dougherty, Space and Atmospheric Physics Group, Imperial College, London SW7 2BZ, UK.

D. C. Hamilton, Department of Physics, University of Maryland, College Park, MD 20742, USA.

N. Krupp, Max-Planck-Institut für Sonnensystemforschung, D-37191 Lindau, Germany.

D. G. Mitchell, E. C. Roelof, and A. M. Rymer, Applied Physics Laboratory, Johns Hopkins University, Laurel, MD 20723, USA.

N. Sergis and S. M. Krimigis, Office for Space Research and Technology, Academy of Athens, Athens, GR-157 73 Greece. (nsergis@phys.uoa.gr)

M. F. Thomsen, Los Alamos National Laboratory, Los Alamos, NM, USA.

D. T. Young, Division of Space Science and Engineering, Southwest Research Institute, San Antonio, TX 78228, USA.